ORNL/CP-95774

for publication in J. Nicholls, ed., *High Temperature Surface Engineering*

The Effect of Platinum on the Growth and Adhesion of α-Al_2O_3 Scales

E. C. Dickey*, B. A. Pint†, K. B. Alexander† and I. G. Wright†

* Department of Chemical and Materials Engineering,
University of Kentucky, Lexington, KY 40506-0046
† Metals and Ceramics Division, Oak Ridge National Laboratory,
P.O. Box 2008, Oak Ridge, TN 37831-6156

Abstract

Cast PtAl and NiPtAl alloys were used as model materials to study the effect of Pt on the oxidation behavior of aluminide bond coats. The addition of Pt improves α-Al_2O_3 scale adhesion in cyclic testing at 1150°C and 1200°C. However, in comparison with aluminides which contain reactive elements (e.g. Zr and Hf), the beneficial effect of Pt was not as great. SEM and TEM analysis of the oxides indicated little effect of the Pt on scale microstructure. Using TEM/EDS analysis, Pt was not detected as a segregant to the alumina grain boundaries grown on PtAl, whereas Zr and Hf have been routinely detected. Also, no sulfur was detected at the PtAl/Al_2O_3 interface. While Pt is somewhat beneficial in cast aluminides, Pt in an aluminide bond coat on a single crystal Ni-base superalloy substrate also may provide additional benefits to the overall oxidation behavior.

Introduction

Thermal barrier coatings (TBCs) have played an important role in increasing the efficiency of turbine engines, because they allow the operating temperatures to be increased substantially while protecting the underlying metallic turbine blade. Ceramic TBCs are applied to the hot section of the turbine engine by plasma spraying (PS) or electron-beam physical (EB-PVD).[1-3] Yttria-stabilized zirconia (YSZ) has emerged as the preferred coating material because of its toughness, low thermal conductivity and relatively high thermal expansion coefficient for a ceramic material. One limitation of YSZ is that it has a very high oxygen diffusivity and therefore provides almost no protection of the underlying alloy from oxidation, necessitating an intermediate oxidation-resistant bond coat. This underlying bond coat must not only provide a barrier to oxidation, but must also be resistant to thermo-mechanical fatigue.

In most cases, the bond coat is designed to form an external, protective α-Al_2O_3 scale during oxidation. However, the interface between the bond coat and the Al_2O_3 scale is a common site of mechanical failure resulting in loss of the YSZ top coat, particularly for EB-PVD TBCs[2-3]. To prevent such spallation, it is imperative to control the bond coat chemistry so that the oxide scales that form are adherent. The two most common classes of bond coats are MCrAlY (M=Ni,Co) and diffusion aluminides. For MCrAlY coatings, Y is added to improve scale adhesion. The effect of reactive elements (REs), like Y, have been extensively studied (see for example reviews in references[4-9]). For the case of aluminides, the addition of Pt is known to improve scale adhesion,[10-15] but there have been no mechanisms proposed in the literature for the beneficial effect of Pt.

This paper presents initial results of a study on the role of Pt in improving scale adhesion in Pt aluminide bond coats. Model Pt-containing alloys, with and without RE additions, were cast and both isothermal and cyclic oxidation studies

DISCLAIMER

were performed on the various bond-coat-type compositions to assess the oxidation behavior. Complementary microstructural and chemical studies were carried out using scanning electron microscopy (SEM), energy-dispersive x-ray spectroscopy (EDS) and scanning transmission electron microscopy (STEM) to gain a better understanding of the role of Pt in improving oxidation resistance.

Experimental Procedure

The chemical composition of the substrates investigated in this study are shown in Table I. The 2.3 at.% (10 wt%) Pt level in the NiPtAl alloys was chosen to approximate the level in a Pt aluminide bond coat. The platinum and nickel aluminides were inductively melted and cast in a copper mold and were then annealed for 4 hr at 1350°C.[16] Generally, test specimens were disks of 12-16 mm diameter and 1-2 mm thick.

Thermal cycling exposures were conducted in two ways: (1) samples were cycled in an automated furnace system at 1150° and 1200°C with dry O_2 flowing through a reaction tube; cycle time (time at temperature) was 1h with 10 min. cooling periods between cycles; and (2) samples were exposed in individual pre-annealed alumina crucibles at 1200°C in laboratory air for 100hr cycles. In both cases, the samples were inserted into a hot furnace but, with the alumina crucibles, heat-up time for the samples was somewhat slower. The crucibles had lids to contain spalled oxide and thus allow the measurement of the total amount of reaction. Isothermal (not cycled) kinetics were measured in dry, flowing O_2 using a Cahn Instruments, Model 1000 microbalance.

After oxidation, microstructural and chemical investigations were performed using a Philips XL30 field-emission scanning electron microscope (SEM) with a light-element energy-dispersive spectrometer (EDS). Selected samples were Cu-plated and cross sectioned, either for metallographic polishing and SEM analysis or

Table I. Chemical composition of the substrate alloys in atomic percent. Compositions were determined by inductively coupled plasma analysis; S, C, O, N by combustion analysis.

Alloys	Undoped NiAl	NiAl + Zr	NiAl +Hf	PtAl	PtAl +Zr	NiPtAl	NiPtAl +Hf	NiPtAl +Hf/Si	René N5
Ni	48.67	50.04	48.83	<0.01	0.02	45.75	45.19	45.02	64.85
Al	51.22	49.65	51.05	49.33	51.58	51.83	52.23	52.25	13.88
Pt				50.32	48.07	2.33	2.36	2.30	
Fe	0.01	0.02	0.03	<0.01		<0.01	<0.01	<0.01	0.08
Cr	<0.01	<0.01	<0.01	0.02		0.01	0.01	<0.01	7.79
Si	0.06	0.21	<0.01	0.04	<0.01	<0.01	<0.01	0.19	0.15
Other	0.004 B	<0.01 Y	<0.01 Y	0.04 Cu	<0.01 Hf <0.001 Y	0.002 Ce	0.002 Ce <0.001 Y <0.01 Zr	0.01 Cu 0.004 B <0.001 Y <0.01 Zr	7.28 Co 2.11 Ta 1.61 W 1.02 Re 0.90 Mo
Dopant	<0.01 Hf <0.001 Y <0.01 Zr	0.04 Zr	0.05 Hf 0.01 Zr	<0.01 Hf <0.001 Y <0.01 Zr	0.04Zr	<0.01 Hf <0.001 Y <0.01 Zr	0.05 Hf	0.06 Hf	0.05 Hf 0.003 Y 0.003 Zr
C	0.04	0.02	0.04	<0.01			0.04	0.04	0.25
O	0.004	0.02	0.003	0.252	0.027	0.072	0.102	0.128	0.005
N	<0.001	n.d.	<0.001	0.005	<0.001	<0.001	0.002	0.003	<0.001
S (ppma)	< 4	47	< 4	< 10	< 12	10	< 4	< 4	7

thinned for higher spatial resolution analysis on a Philips 200 field-emission scanning transmission electron microscope (STEM) equipped with light-element EDS.

Results and Discussion

Cyclic oxidation studies were carried out on NiAl, NiPtAl (10wt%Pt) and PtAl to assess the effect of Pt on the oxidation behavior of aluminides, Figure 1. In 1hr cycles at both 1150°C and 1200°C, the addition of Pt significantly improves spallation resistance as compared to undoped β-NiAl, where weight losses reflect continuous spallation of the alumina scale. However, after longer times in the same tests, spallation was observed for both Pt-containing alloys, Figure 2. The onset of

spallation occurred after approximately 500 1hr cycles at 1150°C and 100-150 cycles at 1200°C.

Comparing the effect of Pt on scale adhesion to that of RE additions such as Zr and Hf clearly indicates that the beneficial effect of RE-doping on scale adhesion is much stronger than that of Pt, Figure 2. Based on the performance of NiAl+Hf compared with NiPtAl+Hf and NiPtAl+Hf/Si, it is evident that Pt is not necessary to achieve good scale adhesion. This is similar to the results found for Pt and Hf additions to CoCrAl alloys[14]. Also, the addition of Si and Hf did not provide any additional benefit to the oxidation behavior of cast NiPtAl. An important aspect of the specimen weight gain data in Figures 2a and 2b is that a simple comparison of the absolute weight gains for the various samples is not necessarily indicative of some important factors. At both temperatures, initial weight gains for both PtAl and NiPtAl are higher than for Zr- and Hf-doped aluminides. This does not reflect better scale adhesion for the Pt-containing aluminides but rather a more rapid scale growth rate without RE-doping[8,9,17,18]. As illustrated in Figure 3, the addition of Zr reduces the parabolic growth rate by a factor of approximately 3, while a Hf addition reduces the rate by a full order of magnitude. (An explanation for the additional benefit of Hf has not yet been determined.) Thus, the higher initial weight gains for the undoped Pt-containing alloys is the result of an adherent but faster growing scale.

Another point to note in Figure 2 is the high weight gains for PtAl -- the final weight gain after 1000, 1-hr cycles at 1200°C was 20.8 $mg \cdot cm^{-2}$. Again, this is not an indication of good performance. The high weight gains are a result of internal cracking and oxidation of the brittle alloy (Figure 4a) which masks any weight loss due to spallation of the external alumina scale. Some alloy cracking may initiate due to casting defects, however, the PtAl+Zr alloy also had casting defects but did not show similar cracking and internal oxidation after cycling, Figure 4b. From the

weight gain curves for PtAl+Zr, it is evident that there was virtually no spallation from this alloy. In the light micrograph, there appears to be a second phase forming near the surface, an approximately 40 μm thick layer formed after 1000, 1-hr cycles at 1200°C, Figure 4b. This Al-depleted Pt-Al phase has not been conclusively identified by XRD, but EDX analysis indicated Pt_5Al_3. The formation of a depleted layer is not surprising as PtAl is a line compound[19]. This outer layer appears cracked and brittle, but this cracking may have occurred during specimen preparation. Because of the severe cracking on the cycled PtAl, it is difficult to compare the depleted areas in that material. Instead, the two Pt aluminides were compared after a 100hr isothermal exposure at 1200°C, Figure 5 (the same samples that were used for kinetic data in Figure 3). Using SEM back-scattered electron imaging (sensitive to substrate atomic number) of the metallographic cross-section, the Al depletion layer near the surface was clearly observed. Some spalling of the scale was observed on PtAl (Figure 5a), but the most important feature is a much thicker depletion zone on PtAl (≈32μm) compared to PtAl+Zr (≈17μm). This is a result of the slower oxidation rate due to Zr doping (Figure 3) which means a slower Al consumption rate and, therefore, less Al depletion. If this Pt_5Al_3 layer is more brittle than PtAl, then the thicker Pt_5Al_3 layer on the undoped PtAl alloy may contribute to internal cracking and the detrimental behavior observed during thermal cycling. Once the alloy cracks, faster oxidation (forming in the cracks) and more depletion will occur. Thus, Zr-doping not only produced a thinner scale (subject to lower strains on cooling[20]) but a thinner depletion layer in the alloy which also may help in preventing the formation of internal cracks. The polished cross-sections also reveal a pore in the PtAl alloy (Figure 5a) with cracks emanating from it -- a type of defect that may nucleate alloy cracks. In addition, the scale and metal-scale interface on PtAl+Zr (Figure 5b) appear more convoluted than on PtAl. This is somewhat surprising because the convoluted scale is more adherent. However, the convolutions do not appear to be

prevalent in the sample cycled for 1000 hr, Figure 4b.

The effect of cycle time on scale adhesion was also investigated by performing complementary 100-hr cycles for 1000 hr at 1200°C, Figure 6. Total weight gains are shown to illustrate the total amount of attack. Surprisingly, with the longer cycle time, the benefit of Pt-doping was almost non-existent. The addition of a RE again overshadowed the Pt effect. The near-linear weight gains for the undoped alloys reflect almost complete spallation. For PtAl, there was less external spallation but increased weight gains due to internal attack. One possible explanation for the reduced effect of Pt after longer cyclic exposures is that Pt doping is unable to prevent the growth of interfacial voids to the same degree as RE-doping. Large interfacial voids were observed in the spalled areas (exposed substrate) of undoped NiPtAl after 10, 100-hr cycles at 1200°C, Figure 7. It may be that although Pt reduces the growth rate of interfacial voids, it does so to a lesser degree than RE-doping. A smaller fraction of interfacial voids should improve scale adhesion, particularly in short time tests, Figure 1. However, at longer times, the voids would be of sufficient size to cause scale spallation. The longer cycle time (100 hr) allows enough time for the voids to grow and results in spallation after each cycle. Thus the benefit of the Pt addition is lost when the cycle time is increased. A reduction in the interfacial void growth rate also could involve an interaction between Pt and the interfacial segregation of indigenous S (which is thought to accelerate the growth of interfacial voids[21,22]). However, a Pt-S interaction has not yet been investigated.

From the cyclic and isothermal oxidation results, it is clear that the beneficial Pt effect results from a significantly different mechanism than the RE effect. One additional element of RE-doping is a change in the α-Al_2O_3 microstructure.[8,9,18,23] A comparison of the scales formed at 1200°C reveals that the addition of Pt did not produce a fully columnar grain structure or inhibit the formation of alumina whiskers, Figure 8. This is in agreement with the assumption that the columnar

structure is the result of a change in the growth mechanism to predominant O diffusion inward.[8,9,23] Platinum did not reduce the scale growth rate (Figure 3), thus it is not likely that it changed the growth mechanism. The whiskers on the scales formed on undoped Pt aluminides are a further indication that outward diffusion of Al is contributing to the scale growth rate, Figure 8.

STEM and EDS analyses were performed on PtAl and PtAl+Zr after oxidation for 2hr at 1200°C. At this time no scale spallation was observed. Figure 9a shows a bright-field TEM image of the Al_2O_3 scale grown on undoped PtAl at 1200°C. EDS spectra (Figure 5b) were acquired from the interior of the Al_2O_3 grains as well as the Al_2O_3 grain boundaries. In these undoped PtAl specimens, no evidence was found for segregation of Pt or impurity elements, such as S, to the grain boundaries. EDS analysis was also performed across the PtAl-Al_2O_3 interface. Figure 10a is a high resolution electron microscopy (HREM) image of this interface. The lattice image shows that the interface is abrupt with no other phases present at the PtAl-Al_2O_3 boundary. EDS profiles, taken across the same boundary in 5nm steps (Figure 10b), show an abrupt chemical transition across the interface. EDS also showed no evidence for impurities, such as S, segregated to the interface.

Similar analytical analyses were performed on the scale formed on PtAl+Zr. Figure 11a is a bright-field TEM image of a portion of the Al_2O_3 scale. EDS spectra (Figure 11b) shows that Zr segregated to the Al_2O_3 grain boundaries. This observation is consistent with numerous previous observation of RE ionic segregation (see literature reviews in references 12 and 24). The interface between the PtAl+Zr and Al_2O_3 scale was also examined by HREM and EDS to look for interphases or segregation at the metal-oxide interface. Figure 12a is an HREM image of the interface between PtAl+Zr and Al_2O_3. As in the undoped case, the metal-oxide interface is free of third phases and appears to be structurally abrupt. EDS profiles taken across the boundary, Figure 12b, show that the interface is

chemically abrupt and that Zr segregation was not detected in this sample. Additional TEM work on the NiPtAl alloys has not yet been completed because these alloys are more brittle and thus more difficult to thin for TEM analysis.

While Pt has not been found to be as effective as RE-doping in improving alumina scale adhesion, the addition of Pt to a bond coat on a Ni-base single-crystal superalloy may benefit the oxide behavior by mechanisms not reproducible in these cast alloys. A comparison using STEM/EDS of the scale grown on uncoated René N5 with that grown on a Pt aluminide-coated René N5 substrate indicated that the scale on the uncoated alloy contained significant amounts of Ta-rich oxide particles, and Ta ions segregated to every α-Al_2O_3 grain boundary[25]. Initial results for the scale formed on the Pt-aluminide bond coat showed far less Ta-rich particles in the scale and little segregation of Ta to the scale grain boundaries. Limiting the outward diffusion of elements such as Ta from the substrate into the external alumina scale may be an additional beneficial effect of Pt when present in an aluminide coating. In general, it has been observed that a small amount of RE-doping is beneficial to oxidation performance, but additional dopants in the scale are detrimental in the long term. Thus, Pt in an aluminide coating may have an additional beneficial effect on oxidation by limiting the diffusion of extraneous elements from the substrate into the alumina scale.

Conclusions

1. The addition of Pt to cast aluminides was found to be beneficial to oxide adhesion but not to the same extent as reactive element (Zr, Hf, etc.) doping.
2. The addition of Pt did not change the α-Al_2O_3 scale growth rate or scale microstructure formed on these alloys.
3. Using STEM/EDS, neither Pt or S was found to segregate to the α-Al_2O_3 grain boundaries or the metal-scale interface on cast PtAl. For the scale on PtAl+Zr, Zr

was observed as a segregant on the α-Al_2O_3 grain boundaries.

Acknowledgments

The authors would like to thank M. Brady, D. Wilson and J. R. DiStefano at ORNL for their comments on the manuscript. T. Geer and J. W. Jones at ORNL assisted with the metallography and TEM sample preparation. J. D. Whittenberger and J. Doychak at NASA Lewis Research Center provided some NiAl substrates. This research was sponsored by the U. S. Department of Energy, Assistant Secretary for Energy Efficiency and Renewable Energy, Office of Industrial Technologies, as part of the Advanced Turbine Systems Program (ORNL program manager, M. A. Karnitz) and by the Division of Materials Sciences under contract DE-AC05-96OR22464 with Lockheed Martin Energy Research Corporation.

References

1. R. A. MILLER, "Oxidation-Based Model for Thermal Barrier Coating Life," *J. Amer. Ceram. Soc.*, 1984, **67**, 517-21.
2. A. BENNETT, "Properties of Thermal Barrier Coatings," *Mat. Sci Tech.*, 1986, **2**, 257-61.
3. S. M. MEIER, D. M. NISSLEY, K. D. SHEFFLER and T. A. CRUSE, "Thermal Barrier Coating Life Prediction Model Development," *J. Eng. Gas Turb. & Power*, 1992, **114**, 258-63.
4. *The Role of Active Elements in the Oxidation Behavior of High Temperature Metals and Alloys* , E. Lang, ed., Elsevier Applied Science, London, 1989.
5. *The Reactive Element Effect on High Temperature Oxidation -- After Fifty Years*, W. E. King, ed., Materials Science Forum **43**, Trans. Tech Publications, Switzerland, 1989.
6. D. P. MOON, "Role of Reactive Elements in Alloy Protection," *Mat. Sci. Tech..*, 1989, **5**, 754-64.
7. A. STRAWBRIDGE and P. Y. HOU, "The Role of Reactive Elements in Oxide Scale Adhesion," *Mat. High Temp.*, 1994, **12**, 177-81.
8. B. A. PINT, A. J. GARRATT-REED and L. W. HOBBS, "The Reactive Element Effect in Commercial ODS FeCrAl Alloys," *Mat. High Temp.*, 1995, **13**, 3-16.
9. B. A. PINT, "Experimental Observations in Support of the Dynamic Segregation Theory to Explain the Reactive Element Effect," *Oxid. Met.*, 1996, **45**, 1-37.

10. E. J. FELTEN, "Use of Platinum and Rhodium to Improve Oxide Adherence on Ni-8Cr-6Al Alloys," *Oxid. Met.*, 1976, **10**, 23-8.
11. E. J. FELTEN and F. S. PETTIT, "Development, Growth, and Adhesion of Al_2O_3 on Platinum-Aluminum Alloys," *Oxid. Met.*, 1976, **10**, 189-223.
12. J. G. FOUNTAIN, F. A. GOLIGHTLY, F. H. STOTT and G. C. WOOD, "The Influence of Platinum on the Maintenance of α-Al_2O_3 as a Protective Scale," *Oxid. Met.*, 1976 **10**, 341-5.
13. D. LOWRIE AND D. H. BOONE, "Composite Coatings of CoCrAlY Plus Platinum," Thin Solid Films, 1977, **45**, 491-8.
14. I. M. ALLAM, H. C. AKUEZUE and D. P. WHITTLE, "Influence of Small Pt Additions on Al_2O_3 Scale Adherence," *Oxid. Met.*, 1980, **14**, 517-30.
15. J. P. ROUX, M. W. BRUMM and H. J. GRABKE, "Effects of Orientation and Doping with Platinum on the Oxidation of β-NiAl," *Fresenius J. Anal. Chem.*, 1993, **346**, 265-8.
16. B. A. PINT and I. G. WRIGHT, "The Effect of Pt on the Oxidation Behavior of Aluminides," manuscript in progress for submission to *Oxid. Met.*
17. B. A. PINT, J. R. MARTIN and L. W. HOBBS, "^{18}O/SIMS Characterization of the Growth Mechanism of Doped and Undoped α-Al_2O_3," *Oxid. Met.*, 1993, **39**, 167-95.
18. B. A. PINT, "The Oxidation Behavior of Oxide-Dispersed β-NiAl: I. Short-Term Performance at 1200°C," *Oxid. Met.*, 1998, in press.
19. *Binary Alloy Phase Diagrams*, 1st edition, T. B. Massalski et al. eds., ASM International, Metals Park, OH, 1986.
20. H. E. EVANS, "Stress Effects in High Temperature Oxidation of Metals," *Int. Mat. Rev.*, 1995, **40**, 1-40.
21. H. J. GRABKE, D. WEIMER and H. VIEFHAUS, "Segregation of Sulfur During Growth of Oxide Scales," *Appl. Surf. Sci.*, 1991, **47**, 243-50.
22. B. A. PINT, "On the Formation of Interfacial and Internal Voids in α-Al_2O_3 Scales," *Oxid. Met.*, 1997, **48**, 303-33.
23. F. A. GOLIGHTLY, F. H. STOTT and G. C. WOOD, "The Relationship Between Oxide Grain Morphology and Growth Mechanisms for Fe-Cr-Al and Fe-Cr-Al-Y Alloys," *J. Electrochem. Soc.*, 1979, **126**, 1035-42.
24. B. A. PINT, A. J. GARRATT-REED and L. W. HOBBS, "A Possible Role of the Oxygen Potential Gradient in Enhancing Diffusion of Foreign Ions on α-Al_2O_3 Grain Boundaries," *J. Amer. Ceram. Soc.*, 1998, **81**, in press.
25. B. A. PINT, I. G. WRIGHT, W. Y. LEE, Y. ZHANG, K. PRÜßNER and K. B. ALEXANDER, "Substrate and Bond Coat Compositions: Factors Affecting Alumina Scale Adhesion," *Mat. Sci. and Eng.*, 1998, in press.

List of Figures

Figure 1. Weight change of various uncoated aluminides cycled (1h cycle time) from room temperature to (a) 1150°C and (b) 1200°C[16]. The addition of Pt improved scale adhesion compared to undoped β-NiAl.

Figure 2. Weight change of various uncoated aluminides cycled (1h cycle time) from room temperature to (a) 1150°C and (b) 1200°C[16]. The addition of reactive elements such as Zr and Hf further improve scale adhesion compared to a Pt addition alone. The high weight gains for PtAl are due to internal cracking and oxidation.

Figure 3. Isothermal weight gains at 1200°C plotted versus the square root of time to show the parabolic reaction kinetics[16]. The addition of Hf reduces the scale growth rate by a factor of 10, while a Zr addition is slightly less effective. This reduction in rate is attributed to an inhibition of Al diffusion in the Zr- or Hf-doped α-Al_2O_3 scale.

Figure 4. a) SEM back-scattered electron image of a metallographically-polished cross-section of PtAl cyclically oxidized at 1200°C for 1000 1-hr cycles, b) light micrograph of PtAl+Zr after the same test. Without the reactive element (Zr) addition, massive cracking and internal oxidation occurs. A depletion layer is observed in the PtAl+Zr near the scale.

Figure 5. Cross sectional SEM back-scattered images of a) PtAl and b) PtAl+Zr after isothermal oxidation at 1200°C for 100 hr. Spallation of the Al_2O_3 scale is apparent in the undoped PtAl, while the scale is well adhered in the Zr-doped specimen. The slower scale growth rate with Zr doping also results in a much thinner Pt_5Al_3 layer. The arrows in (a) mark a void with cracks near it.

Figure 6. Total weight gain (sample weight gain + spalled oxide) during 100hr cycles at 1200°C. The nearly straight line behavior of undoped NiAl represents almost complete spallation during cooling after each cycle. The addition of Pt had only a marginal effect on adhesion in this longer term cyclic test. However, the addition of Hf or Zr continues to provide a benefit throughout the test with almost no spallation observed.

Figure 7. SEM secondary electron image of the NiPtAl (10wt%Pt) substrate exposed by spallation of the alumina scale after 10, 100hr cycles at 1200°C. The arrows mark a variety of large voids.

Figure 8. SEM secondary electron cross-section images of the α-Al_2O_3 scale formed at 1200°C on (a) undoped NiPtAl after 100h, (b) β-NiAl + Hf after 100h, (c) PtAl after 100hr and (d) NiPtAl+Hf after 100hr[16]. With the additional of a reactive element such as Hf, the oxide whiskers disappear and a more columnar grain structure develops.

Figure 9. a) Bright-field TEM image of isothermally-grown Al_2O_3 scale on PtAl and b) EDS spectra from Al_2O_3 grains and grain boundary showing no segregation to the grain boundaries. Note that the spectra intensities are offset for clarity. The Cu, Pt and Ar peaks are artifacts from sample preparation.

Figure 10. a) HREM image of PtAl - Al_2O_3 interface in isothermally oxidized (1200°C, 2hr) PtAl sample and b) EDS profiles taken across the interface which show an abrupt transition between the metal and oxide scale.

Figure 11. a) Bright-field TEM image of columnar alumina scale on isothermally oxidized PtAl+Zr and b) EDS spectra from alumina grains and grain boundary showing segregation of Zr to grain boundaries. The intensities of the three spectra are offset for clarity. Traces of Pt are also detected in the alumina grains and grain boundaries.

Figure 12. a) HREM image of PtAl+Zr -Al_2O_3 interface in isothermally oxidized (1200°C, 2hr) PtAl+Zr sample and b) EDS profiles taken across the interface which show an abrupt chemical transition between the metal and oxide scale.

a

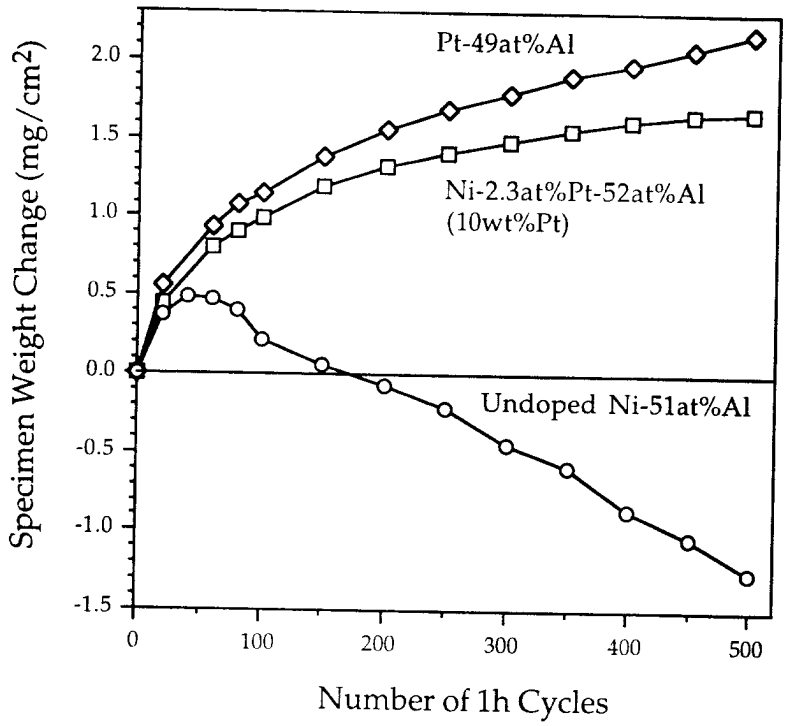

b

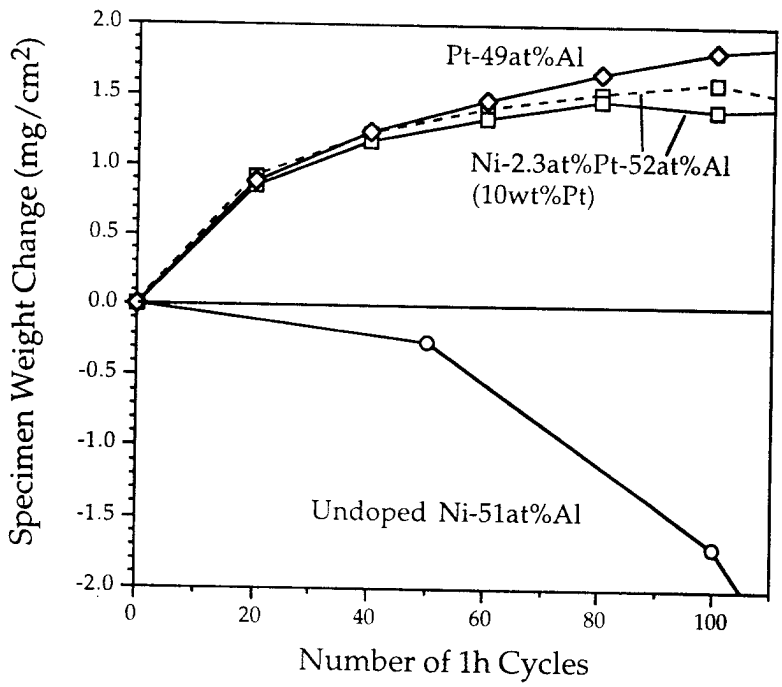

Figure 1. Weight change of various uncoated aluminides cycled (1h cycle time) from room temperature to (a) 1150°C and (b) 1200°C[16]. The addition of Pt improved scale adhesion compared to undoped β-NiAl.

a

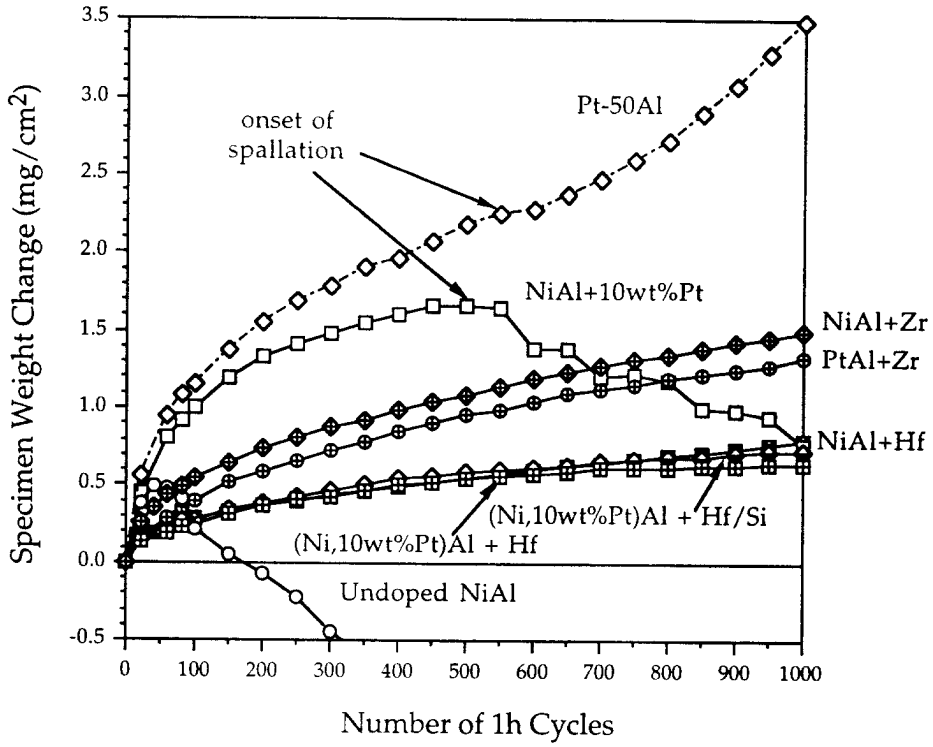

b

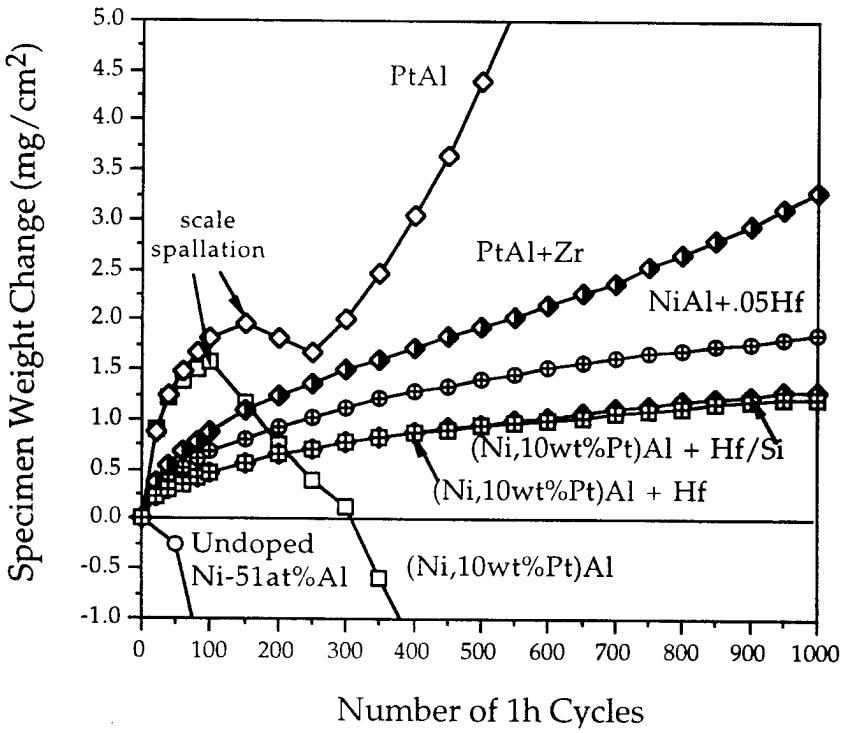

Figure 2. Weight change of various uncoated aluminides cycled (1h cycle time) from room temperature to (a) 1150°C and (b) 1200°C[16]. The addition of reactive elements such as Zr and Hf further improve scale adhesion compared to a Pt addition alone. The high weight gains for PtAl are due to internal cracking and oxidation.

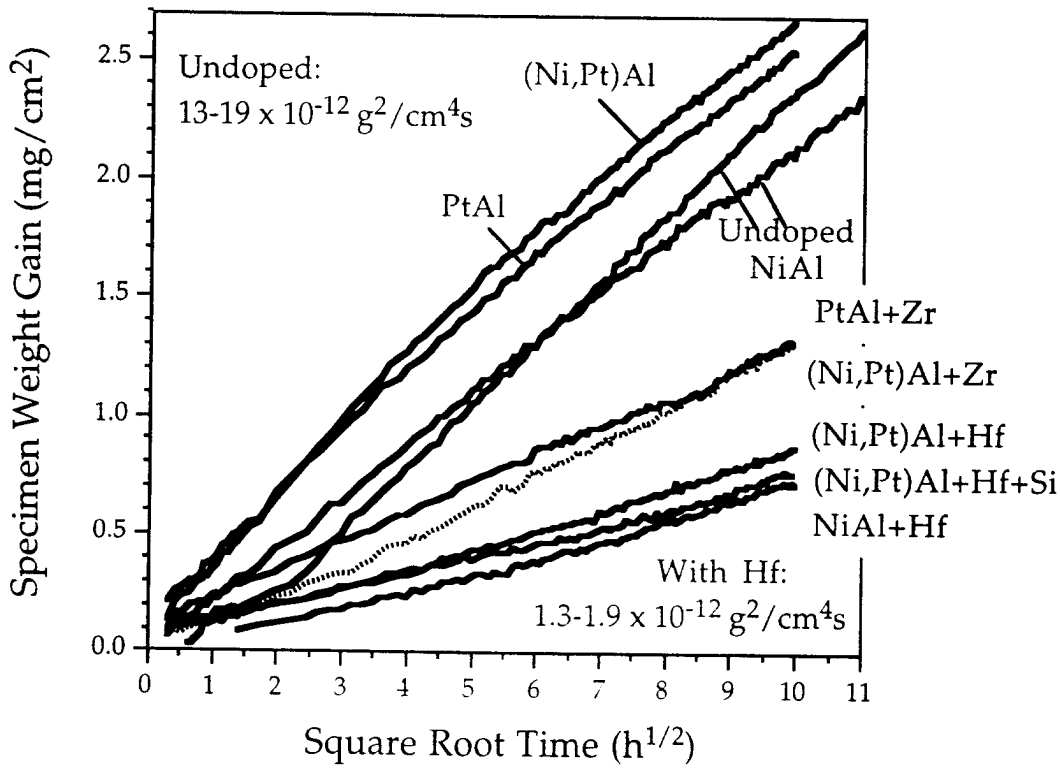

Figure 3. Isothermal weight gains at 1200°C plotted versus the square root of time to show the parabolic reaction kinetics[16]. The addition of Hf reduces the scale growth rate by a factor of 10, while a Zr addition is slightly less effective. This reduction in rate is attributed to an inhibition of Al diffusion in the Zr- or Hf-doped α-Al_2O_3 scale.

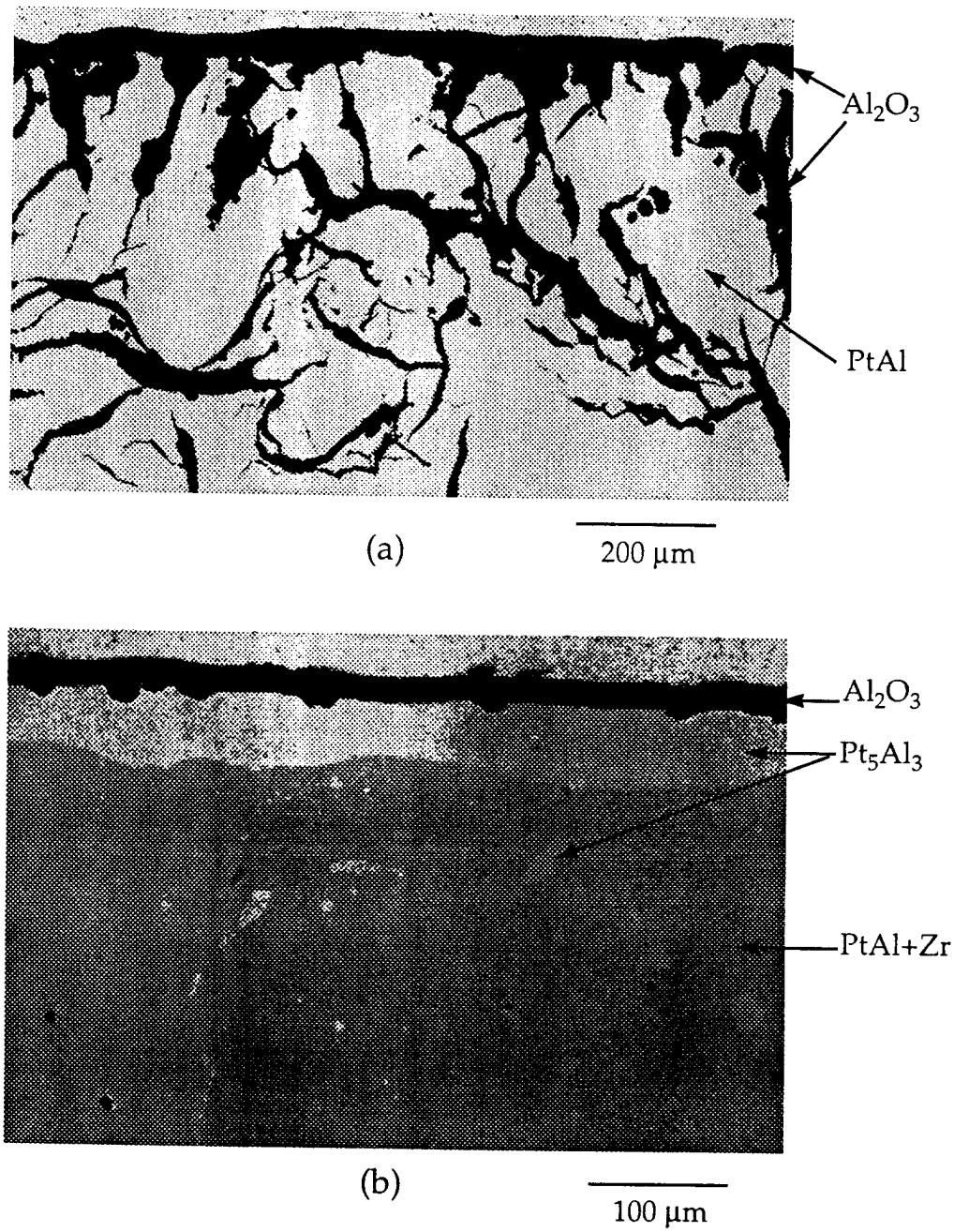

Figure 4. Light micrographs of metallographically-polished cross-sections of (a) PtAl and (b) PtAl+Zr, after 1000 1-hr cycles at 1200°C. Without the reactive element (Zr) addition, massive cracking and internal oxidation occurs. A depletion layer is observed in the PtAl+Zr near the scale.

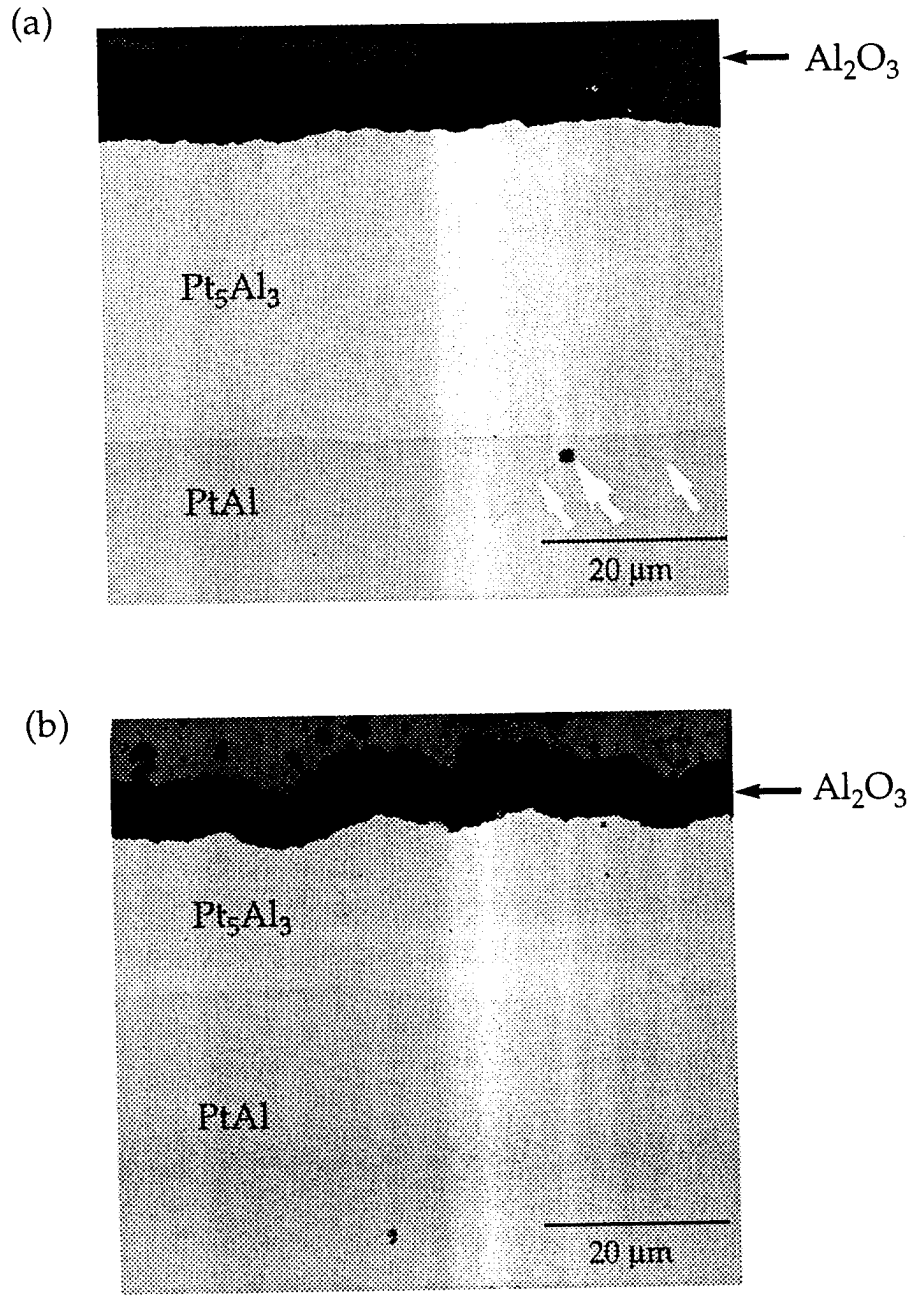

Figure 5. Cross sectional SEM back-scattered images of a) PtAl and b) PtAl+Zr after isothermal oxidation at 1200°C for 100 hr. Spallation of the Al_2O_3 scale is apparent in the undoped PtAl, while the scale is well adhered in the Zr-doped specimen. The slower scale growth rate with Zr doping also results in a much thinner Pt_5Al_3 layer. The arrows in (a) mark a void with cracks near it.

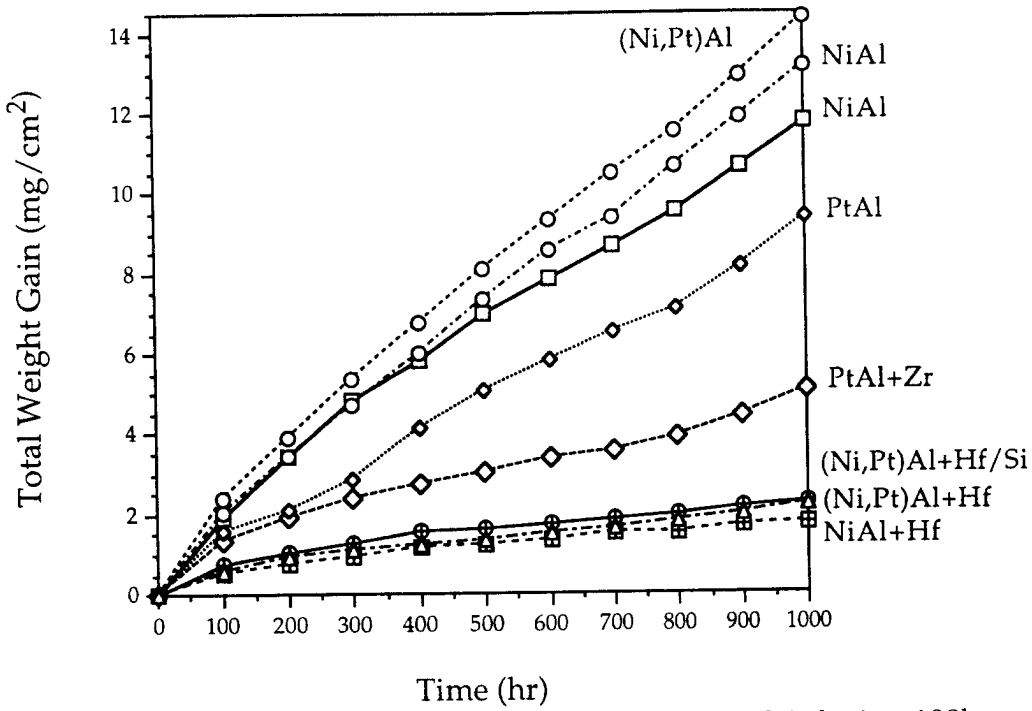

Figure 6. Total weight gain (sample weight gain + spalled oxide) during 100hr cycles at 1200°C. The nearly straight line behavior of undoped NiAl represents almost complete spallation during cooling after each cycle. The addition of Pt had only a marginal effect on adhesion in this longer term cyclic test. However, the addition of Hf or Zr continues to provide a benefit throughout the test with almost no spallation observed.

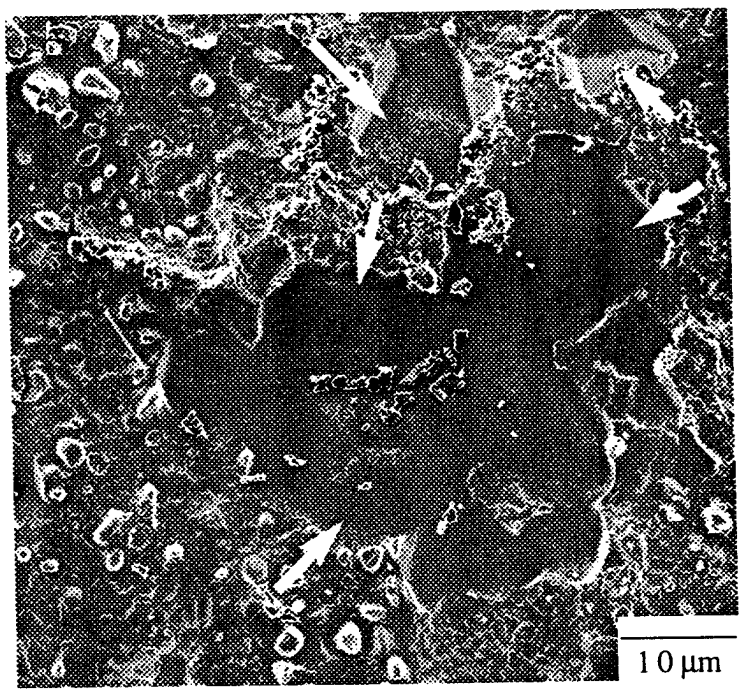

Figure 7. SEM secondary electron image of the NiPtAl (2.3at.%, 10wt%Pt) substrate exposed by spallation of the alumina scale after 10, 100hr cycles at 1200°C. The arrows mark a variety of large voids.

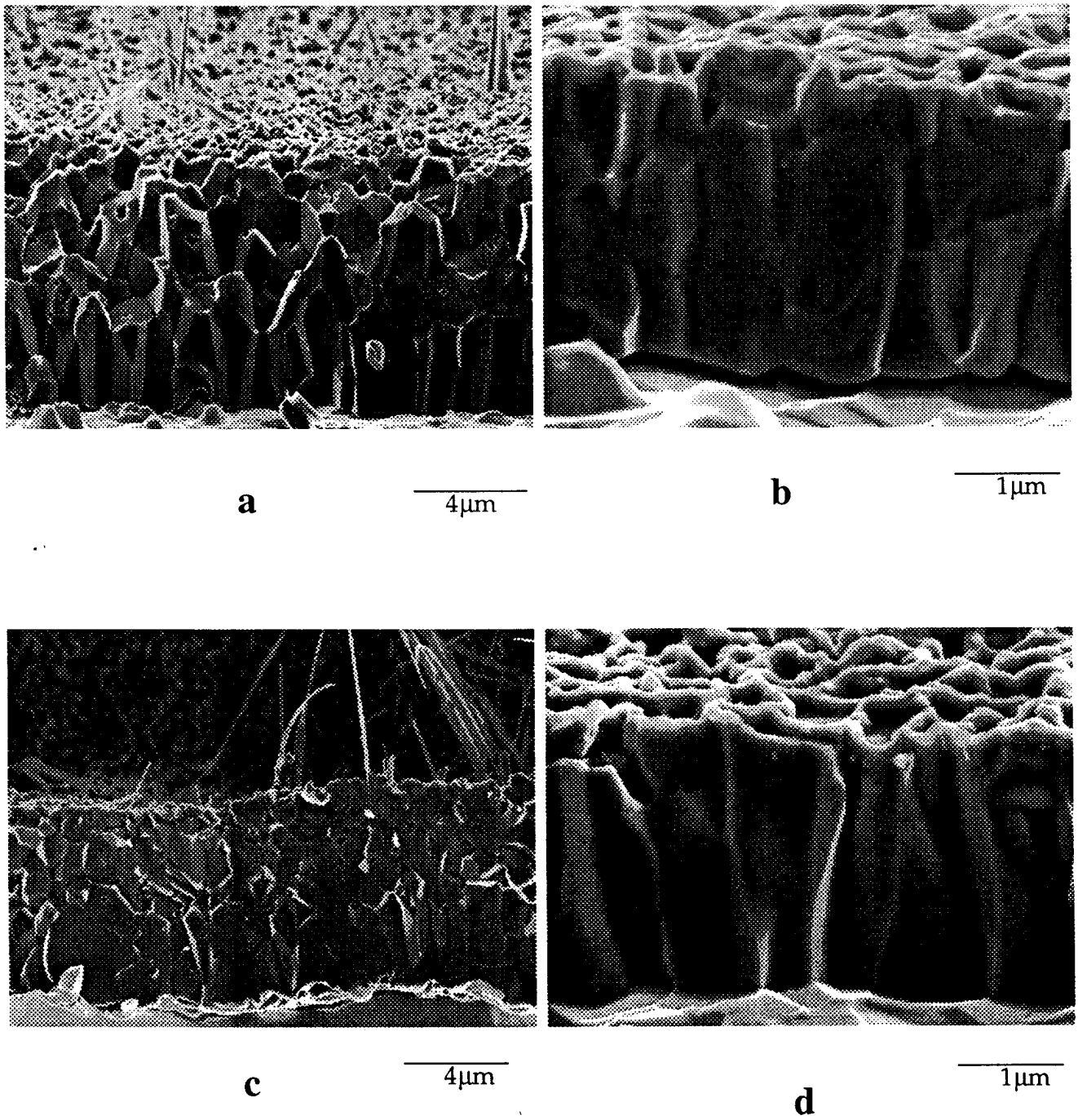

Figure 8. SEM secondary electron cross-section images of the α-Al_2O_3 scale formed at 1200°C on (a) undoped NiPtAl after 100h, (b) β-NiAl + Hf after 100h, (c) PtAl after 100h and (d) NiPtAl+Hf after 100h[16]. With the additional of a reactive element such as Hf, the oxide whiskers disappear and a more columnar grain structure develops.

(a)

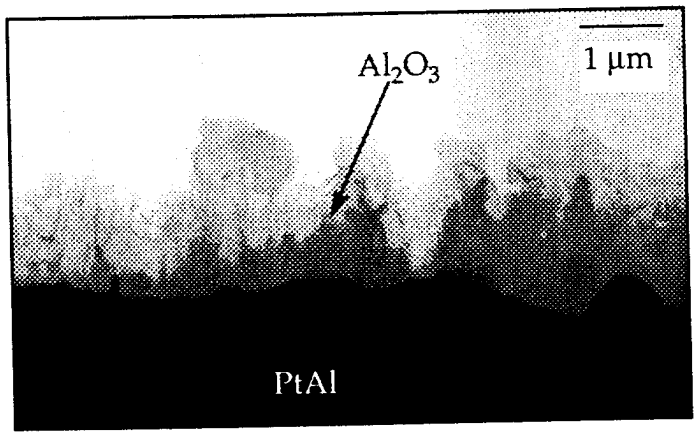

(b)

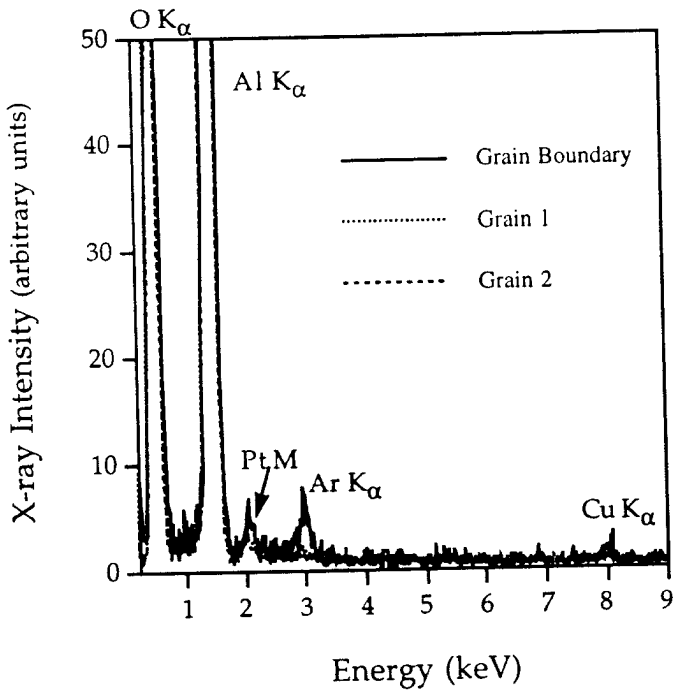

Figure 9. a)Bright-field TEM image of isothermally-grown Al_2O_3 scale on PtAl and b) EDS spectra from Al_2O_3 grains and grain boundary showing no segregation to the grain boundaries. Note that the spectra intensities are offset for clarity. The Cu, Pt and Ar peaks are artifacts from sample preparation.

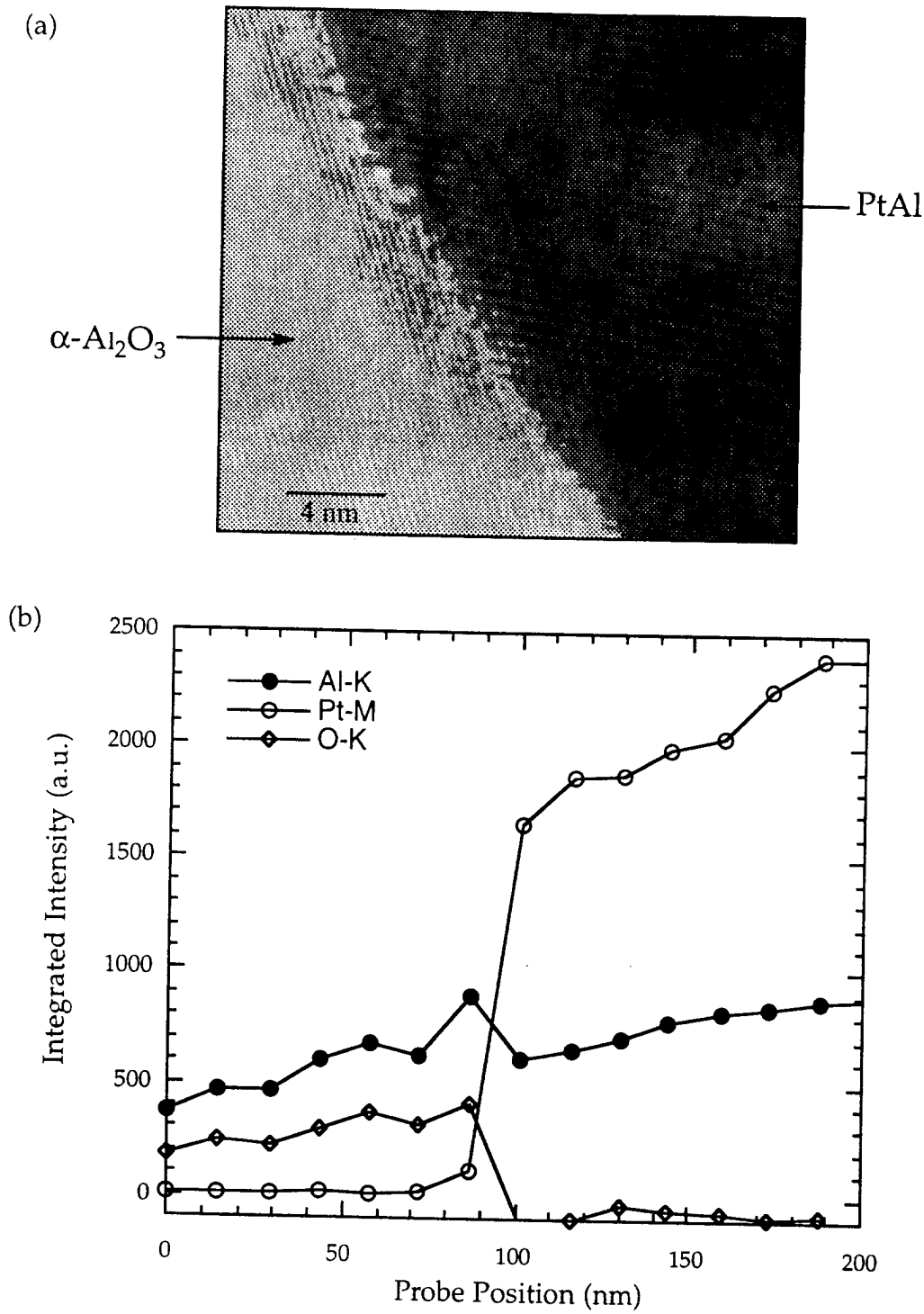

Figure 10. a) HREM image of PtAl - Al_2O_3 interface in isothermally oxidized (1200°C, 2hr) PtAl sample and b) EDS profiles taken across the interface which show an abrupt transition between the metal and oxide scale.

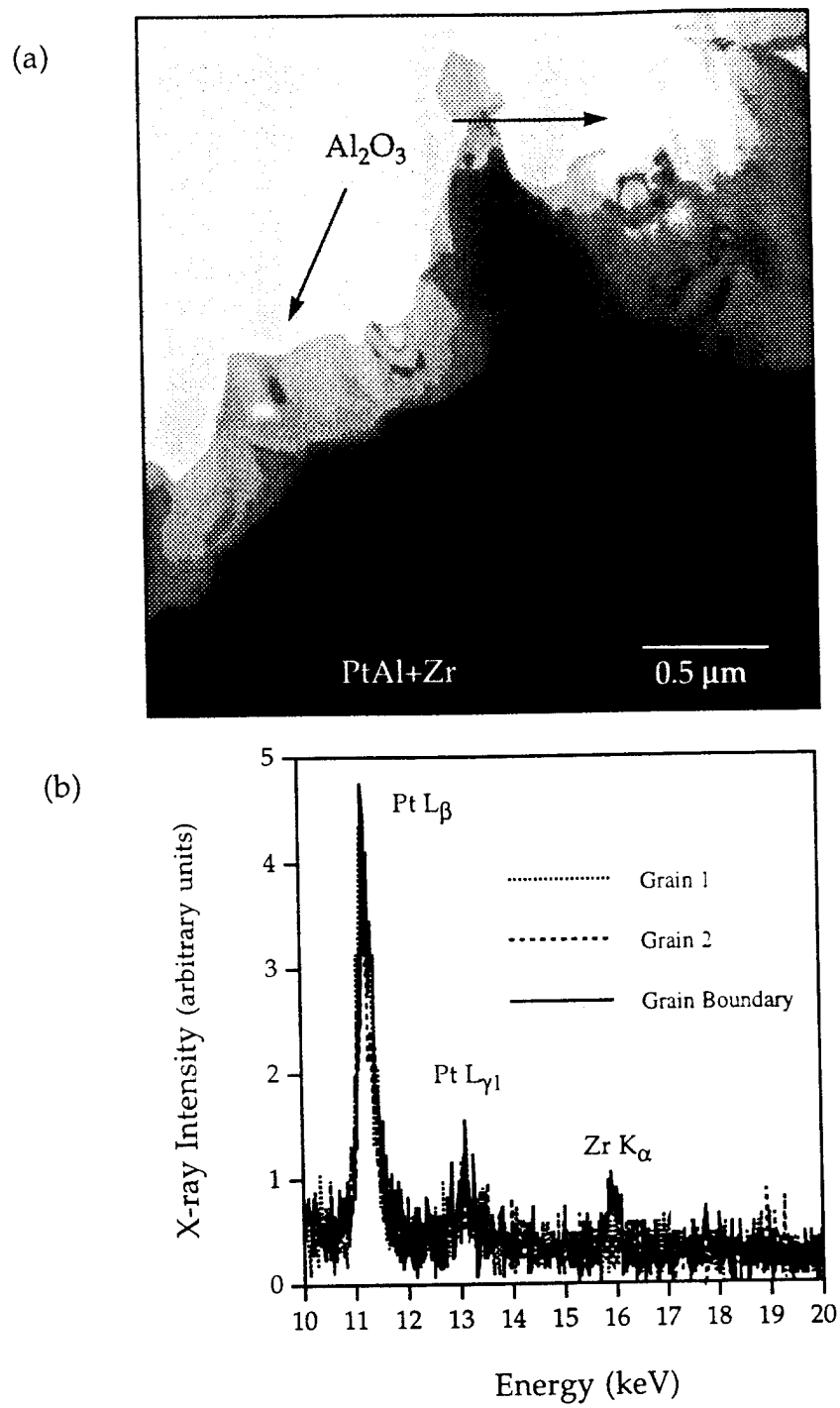

Figure 11. a) Bright-field TEM image of columnar alumina scale on isothermally oxidized PtAl+Zr and b) EDS spectra from alumina grains and grain boundary showing segregation of Zr to grain boundaries. The intensities of the three spectra are offset for clarity. Traces of Pt are also detected in the alumina grains and grain boundaries.

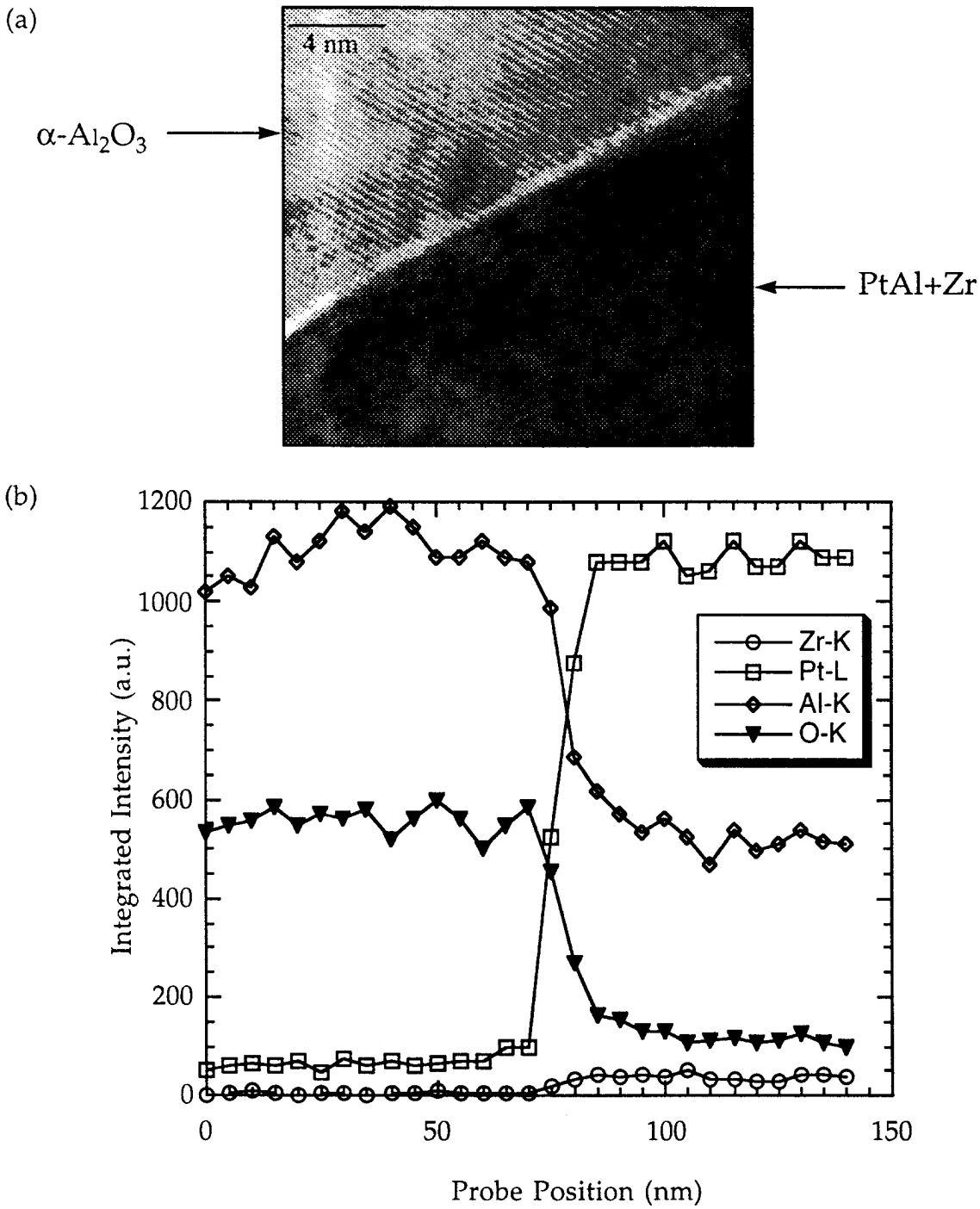

Figure 12. a) HREM image of PtAl+Zr -Al_2O_3 interface in isothermally oxidized (1200°C, 2hr) PtAl+Zr sample and b) EDS profiles taken across the interface which show an abrupt chemical transition between the metal and oxide scale.

Report Number (14) ORNL/CP--95774
CONF-9709183--

Publ. Date (11) 19972
Sponsor Code (18) DOE/ER, XF
JC Category (19) UC-400, DOE/ER

DOE